Journal of Alloys and Compounds 506 (2010) 715–720

Contents lists available at ScienceDirect

Journal of Alloys and Compounds

journal homepage: www.elsevier.com/locate/jallcom

Mechanically activated synthesis of single crystalline MgO nanostructures

M. Nusheh [a,*], H. Yoozbashizadeh [a], M. Askari [a], H. Kobatake [b], H. Fukuyama [b]

[a] Material Science and Engineering Department, Sharif University of Technology, Azadi Street, 11155-9466 Tehran, Iran
[b] Institute of Multidisciplinary Research for Advanced Materials, Tohoku University, 2-1-1 Katahira, Aoba-ku, Sendai 980-8577, Japan

ARTICLE INFO

Article history:
Received 25 April 2010
Received in revised form 4 July 2010
Accepted 7 July 2010
Available online 16 July 2010

Keywords:
Nanostructured materials
Mechanical alloying
Kinetics
Scanning electron microscopy
Transmission electron microscopy

ABSTRACT

One-dimensional (1D) MgO structures were successfully synthesized via carbothermic reduction of mechanically activated mixture of MgO and graphite. Mechanical activation of source materials before carbothermic reduction can substantially enhance the formation of MgO products at a temperature (1000 °C) relatively lower than that required in previous approaches (≥1200 °C). However, the morphology of MgO formed is dependent on the degree of mechanical activation and the condition of the subsequent carbothermic reduction. Two distinctive morphologies were found for MgO products synthesized using our method: single crystalline nanorods with rectangular cross-sections whose diameters range from 50 to 100 nm, and microfibers (~5 μm in diameter) with and without branching. The synthesized products were systematically studied by XRD, SEM, TEM, and EDS. The results show that the nucleation and growth process of these morphologies seem to be a vapor–solid mechanism.

1. Introduction

Magnesium oxide (Periclase) is a typical wide-band-gap insulator. It has found many important applications for use in catalysis, toxic waste remediation, refractory materials, paint, and superconductors. Due to the high-melting point (~2830 °C), high corrosion-resistance and low heat capacity, MgO is very appropriate for insulation applications, especially in steel manufacturing. Its crystals are valuable, e.g., as in optical transmitters and as a good substrate for epitaxial growth of thin films [1]. Another notable application for magnesium oxide is as an agent in the detection and remediation of chemical waste and warfare agents [2].

In recent years, one-dimensional (1D) MgO nanostructures have shown great potential in diverse applications [3]. For instance, these nanostructures have drawn special attention due to their unique ability to reinforce high-temperature superconductor composites (HTSC), by pinning the magnetic flux lines and improving the mechanical properties [4]. Until now, a variety of MgO nanostructures have been successfully synthesized via vapor routes, such as nanorods or nanowires [5,6], fishbone fractal structures [7], nanobelts [8–10], nanotubes [11], nanosheets, nanowhiskers [12], Ga-filled nanotubes [13], Ga_2O_3-filled nanotubes [14], multi-dimensional entities [15–19] and orthogonally branched nanostructures [20].

The source material has a great role in the synthesis of MgO nanostructures. Different MgO nanostructures have been synthesized by vapor phase precursor method using volatile compounds like MgB_2 [5], Mg_3N_2 [16,21] and $MgCl_3$ [8]. Earlier attempts [22,23] at synthesizing MgO nanostructures by directly heating MgO powders required very high temperature (1850 °C) for generating sufficiently high partial pressures of MgO vapor. Yang and Lieber [4] reduced the processing temperature to ~1200 °C by employing a solid mixture of MgO and graphite as the source of the MgO vapor. In this case, Mg with much lower melting point (~650 °C) relative to MgO was produced through the carbothermic reduction of MgO by graphite (Reaction (1)). The Mg vapor subsequently reacted with trace oxygen to generate MgO vapor in the reaction vessel. The carbothermic reaction is:

$$MgO_{(s)} + C_{(s)} = Mg_{(g)} + CO_{(g)} \quad (1)$$

This reaction is favored at very high temperatures and a total product gas pressure of 101 kPa is achieved at 1764 °C [24]. The equilibrium partial pressure of magnesium is shown in Fig. 1.

It is well known that during MgO crystal growth from the vapor, the partial pressure of magnesium vapor or the MgO supersaturation ratio has an important effect on the morphology of the grown crystal [18–20]. As concentration of magnesium vapor increases, the grown crystal will in turn take the form of a one-dimensional fiber, two-dimensional plate, block and eventually a spheroidal particle.

In related studies [25,26], we have conducted a detailed investigation on changes of crystal structures and microstructures of MgO and graphite powder mixtures induced by high-energy milling

* Corresponding author. Tel.: +98 21 66165257; fax: +98 21 66005717.
E-mail addresses: nusheh@mehr.sharif.ac.ir, m_nusheh@yahoo.com (M. Nusheh).

0925-8388/$ – see front matter © 2010 Elsevier B.V. All rights reserved.
doi:10.1016/j.jallcom.2010.07.049

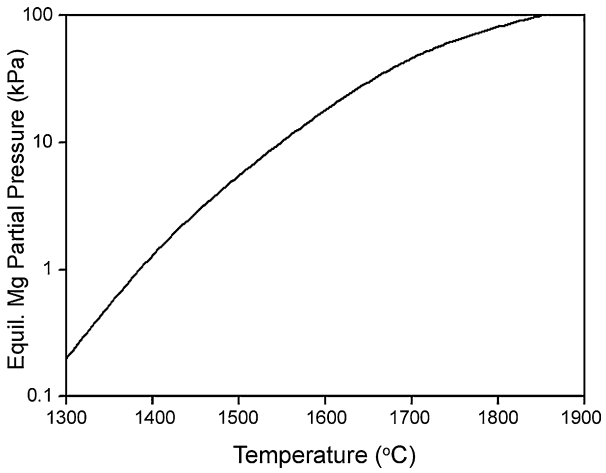

Fig. 1. The partial pressure of magnesium associated with the equilibrium of Reaction (1) [24].

and the effect of these changes on the reactivity of the reactants. Mechanical activation induced by high-energy milling before carbothermic reduction has led to substantial changes in the structural and energy states of the reactants, which in turn increases the reactivity of the reactants. In this study, we focused on the products and investigated effects of the degree of mechanical activation during carbothermic reduction on the nature of the MgO products. At the same time, the growth mechanism of these products was also investigated.

Table 1
Notation of samples in different conditions.

Samples[a]	Milling duration (h)	Molar ratio (MgO:C)	MgO crystallite size[b] (nm)
MG0	0 (unmilled)	1:1	51.14
MG1	1	1:1	24.89
MG8	8	1:1	15.34

[a] *M*: > 99.9 pct MgO, 0.2 μm particle size; *G*: > 98 pct graphite, 45 μm particle size, provided by Wako Chemicals, Japan.
[b] The size of MgO crystallites was determined based on XRD peak broadening using the Scherrer formula.

2. Experimental procedure

The mixture of MgO and graphite was mechanically activated using a planetary ball mill for different durations. Another mixture which was loaded in the mill with no balls and run for several hours, was considered to be physically well mixed and was called the unmilled sample. The notations of samples in different conditions were determined for convenience as shown in Table 1 (e.g. MG8: MgO and graphite mixture was milled for 8 h). Additional details about the preparation of mechanically milled samples are described elsewhere [26].

The experimental setup employed in this research is illustrated in Fig. 2. The system consists of a vertical infrared irradiation furnace (ULVAC, connected to a vacuum system) and a quartz-tube reactor. Firstly, a portion of the samples was placed at the center of a graphite crucible, and the crucible was inserted into the quartz-tube reactor in the IR furnace. An alumina (sapphire) substrate was positioned upstream of the crucible to collect the experimental product (Fig. 2, insets). After the entire system had been evacuated by continuous pumping (with a mechanical pump) for ~10 min, the furnace was heated to 400 °C at a programmed rate of 20 °C/min, and then held at this temperature for ~10 min. At this point, high-purity argon was introduced into the quartz tube at a constant flow rate of 100 ml/min, and the temperature of the furnace was rapidly ramped to the desired temperature (1000 °C). After the furnace had been held at this temperature for ~1 h, the system was cooled down to room temperature at a rate of ~10 °C/min.

At the desired temperature (1000 °C), the white wool-like products were formed in high yield on the surface of the alumina substrate by heating the mechanically

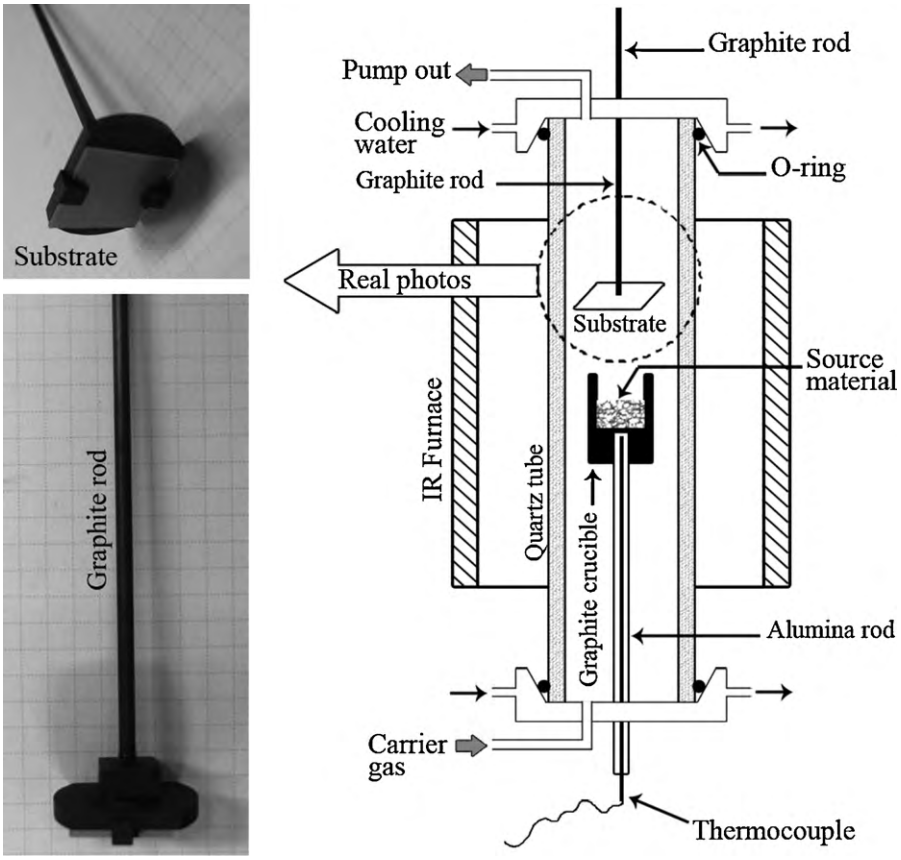

Fig. 2. Schematic diagram of the apparatus used in this work.

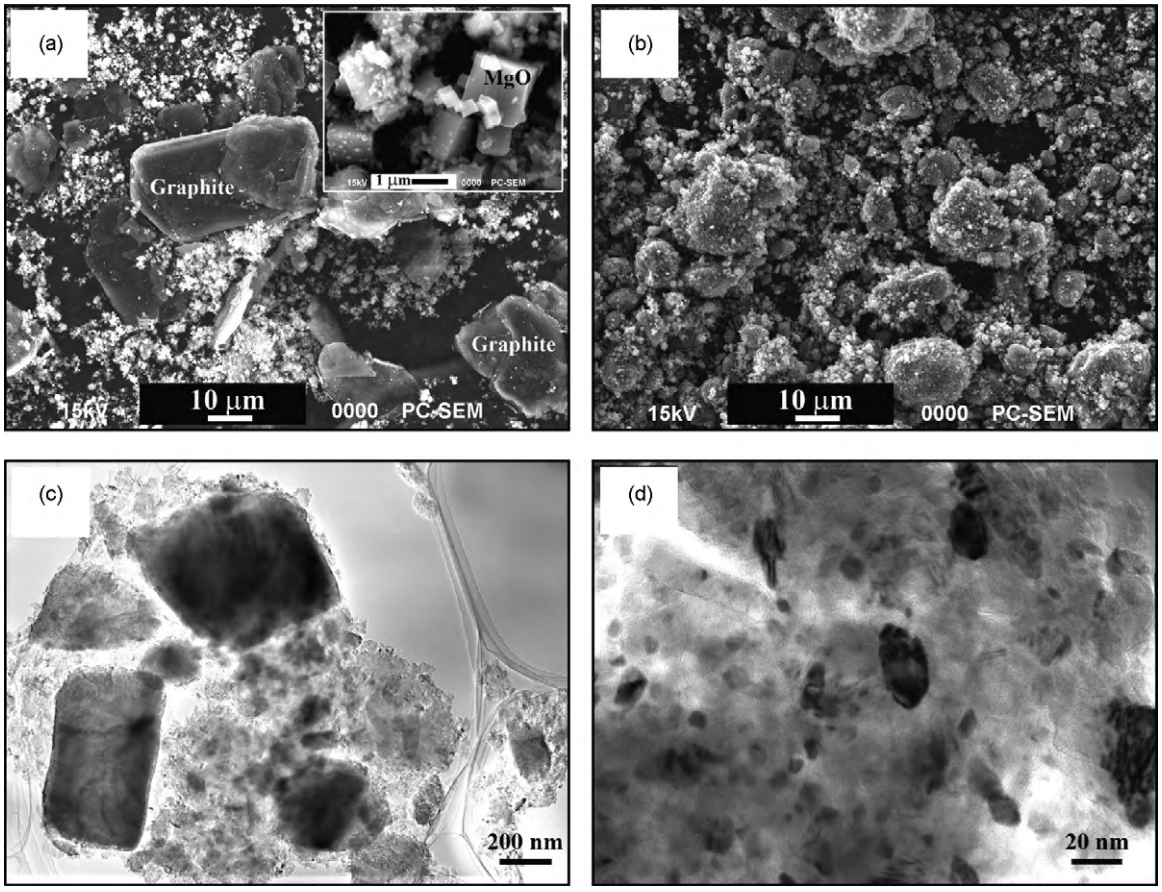

Fig. 3. (a) SEM image of MG0 sample, inset: higher magnification of MG0 sample indicating primary MgO particles. (b) SEM image of MG1 sample. (c) TEM image of MG1 sample. (d) TEM image of MG8 sample.

milled samples (MG1 and MG8); however, no such depositions were found on the alumina substrate when the unmilled sample (MG0) was used at this temperature, as confirmed using SEM. The products were characterized and analyzed by X-ray diffraction (XRD; Rigaku RINT-2000/PC with Cu Kα radiation), scanning electron microscopy (SEM; JEOL JCM-5700) equipped with X-ray energy dispersive spectrometer (EDS) and transmission electron microscopy (TEM; JEOL JEM-3010).

3. Results and discussion

3.1. Characterization of the source materials

The SEM and TEM micrographs of unmilled and milled powders are shown in Fig. 3. The starting powder of MgO consisted of cubic shaped particles of 0.2 μm in average size (Fig. 3a, inset). As evident in Fig. 3a–d, milling resulted in a progressive microstructural refinement of the MgO/graphite powder mixture. Apparently, the massive and compact agglomerates form after 1 h of milling (Fig. 3b). For short milling times, the powder consisted mainly of large particles of similar sizes to the original powder; however, deformation at particle edges and the formation of nanosized grains was evident, as shown in Fig. 3c for a sample milled for 1 h. The proportion of nanocrystalline particles increased with increasing milling time. Samples milled for 8 h or longer consisted entirely of nanocrystalline agglomerates, with crystallite sizes being approximately 5–20 nm, as shown in Fig. 3d. These observations suggest that the milled nanocrystalline particles consisted of composite particles/agglomerates of MgO and graphite and that mixing and contact between the two constituents occurred at the scale of the crystallite size. A higher reaction kinetic is anticipated from these morphological changes.

3.2. Characterization of the products

The products were first characterized by XRD to reveal the overall crystal structure and phase purity of them. Fig. 4 displays the XRD pattern of the wool-like products as prepared. Miller indices are indicated on each diffraction peak. It can be seen that all of the peaks can be indexed in peak position as a face-centered cubic structure of MgO with lattice constant of $a = 0.421$ nm, which is consistent with that of the bulk MgO crystal (JCPDS 4-829).

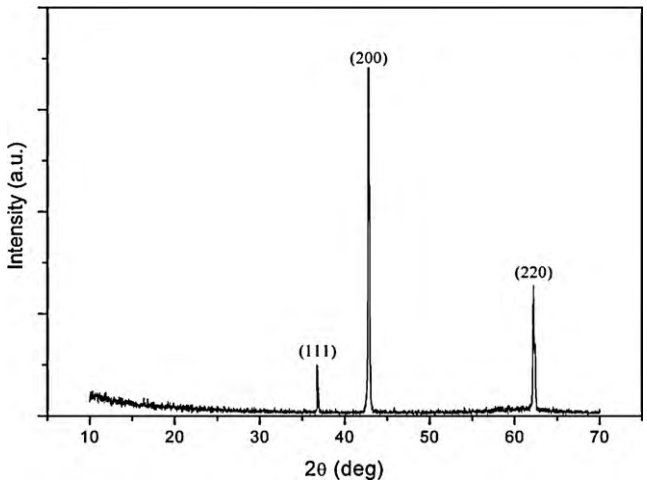

Fig. 4. XRD pattern of the as-prepared wool-like products.

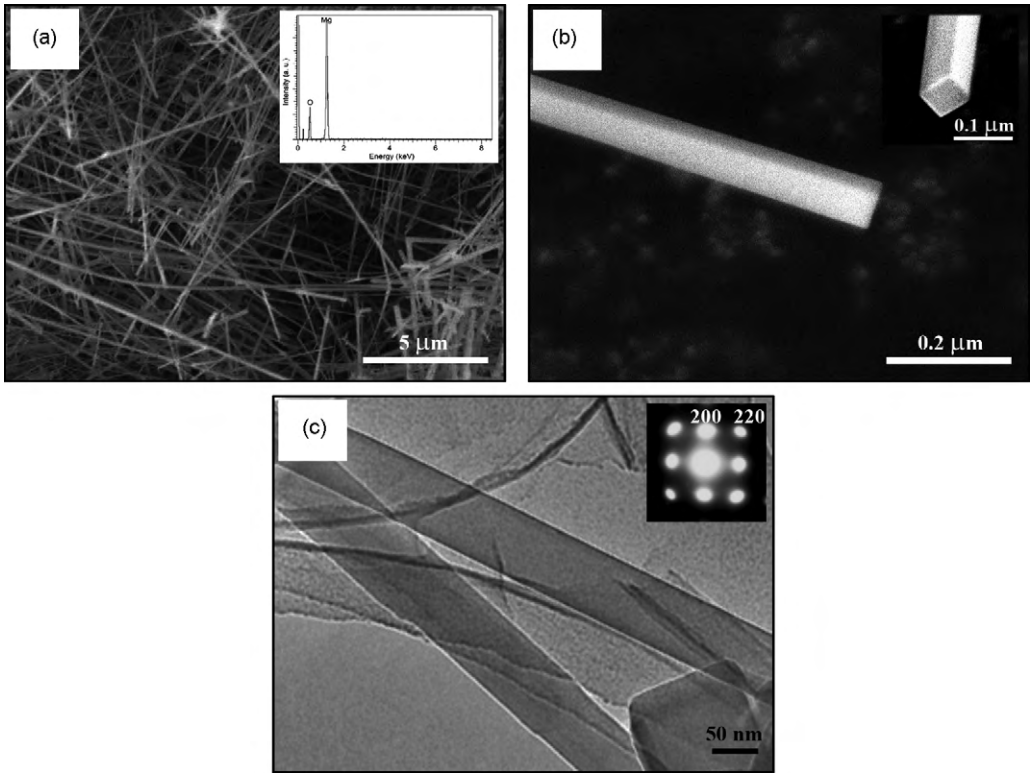

Fig. 5. (a) SEM image of nanorods obtained from MG1 sample; inset: the corresponding EDS spectrum. (b) A higher magnification SEM image of a single nanorod; inset: the rectangular end of the nanorod. (c) TEM image of these MgO nanorods after being transferred onto a carbon grid; inset: the corresponding SAED pattern.

Fig. 5a shows a typical SEM image of the bulk needle-like product formed on the substrate by heating the MG1 sample. The dominant morphology on alumina substrate is randomly distributed nanorods without branching. The composition of the nanorods was confirmed by EDS (Fig. 5a, inset). EDS data recorded on nanorods show that these nanorods mainly consist of Mg and O, and further quantitative analysis shows that the atomic ratio of Mg:O is nearly 1:1, confirming the results of bulk XRD analysis. Rectangular cross-section morphology of a nanorod clearly appears in the higher magnification image (Fig. 5b and its inset), which is believed to be a consequence of the crystallographic symmetry of cubic MgO. Analyses of TEM micrographs recorded on nanorods cleaved from substrate surfaces and dispersed onto holey carbon grids (e.g., Fig. 5c) show that the diameters of these rods range from 50 to 100 nm. The lengths of the rods range from several to tens of micrometers. The rods thus have quite high aspect ratios. The nanorods also appear to have smooth surfaces and may be gently curved. The inset of Fig. 5c is a selected-area electron diffraction (SAED) pattern of the nanorod. The SAED patterns are recorded with the electron beam perpendicular to the long axis of the nanorod and can be indexed to the reflection of the [0 0 1] zone axis. It indicates that the MgO nanorods are single crystalline.

Fig. 6a–d shows the SEM images of the products formed on the substrate by heating the MG8 sample, which shows that it consists of long and branchy fibers. Their lengths reach up to hundreds of micrometers. Similar to the nanorods, EDS also shows that these fibers are mainly composed of Mg and O with atomic ratio of 1:1 (Fig. 6a, inset). Fig. 6b shows that some of these fibers also branched out and grew in various orientations. The angle between the main fiber (stem) and its branches was ~90° in most cases, as determined by cubic symmetry of solid MgO. The diameter is about 5 μm, which is much larger than that of nanorods produced from MG1 sample. The inset in Fig. 6b reveals that these fibers have a rectangular cross-section with a pyramid-shape tip. An enlarged image (Fig. 6c) clearly shows a fiber of which the surface is rather rough by the formation of many short branches at the beginning of their growth, which makes it a camphor tree stalk-like object. For these camphor tree stalk-like MgO fibers, the branches should be related from the secondary crystal growth on the surface of formed main fiber. In some cases, the growth of these sub-branches will be enhanced, resulting in structures similar to fishbone or fern (Fig. 6d). Fig. 6e shows a transmission electron microscopy (TEM) image of an individual fiber with sub-branches that was transferred from the alumina substrate onto a TEM grid.

3.3. Growth mechanism

Several mechanisms have been proposed to account for the growth of 1D structures. The vapor–liquid–solid (VLS) mechanism and the vapor–solid (VS) mechanism are usually used to explain the growth of these structures. The key feature for the VLS growth is that one end of a one-dimensional nanostructure is capped with an alloy droplet promoting the anisotropic crystal growth [27]. Since no sphere-like particles were observed by TEM or SEM at the ends of all of the MgO fibers or nanorods, they were not generated through the VLS mechanism. Also, in our experiment, no transition metal was employed as a catalyst, which is different from previously reported procedures for the formation of other nanostructures. We believe the growth of MgO nanorods and micro fibers in our synthesis simply followed the VS mechanism analogous to that described previously for micron diameter whiskers [28].

MgO is a cubic crystal, possessing relatively isotropic structure in nature. The formation of extremely anisotropic MgO structures is found to be steered by pertinent defects, such as ledges, steps, and kinks [29], which guide the axial growth. Meanwhile, supersaturation ratios in the reaction systems make a remarkable effect on the final architectures, and the growth behaviors of various architectures are manifested kinetically [20]. The different mor-

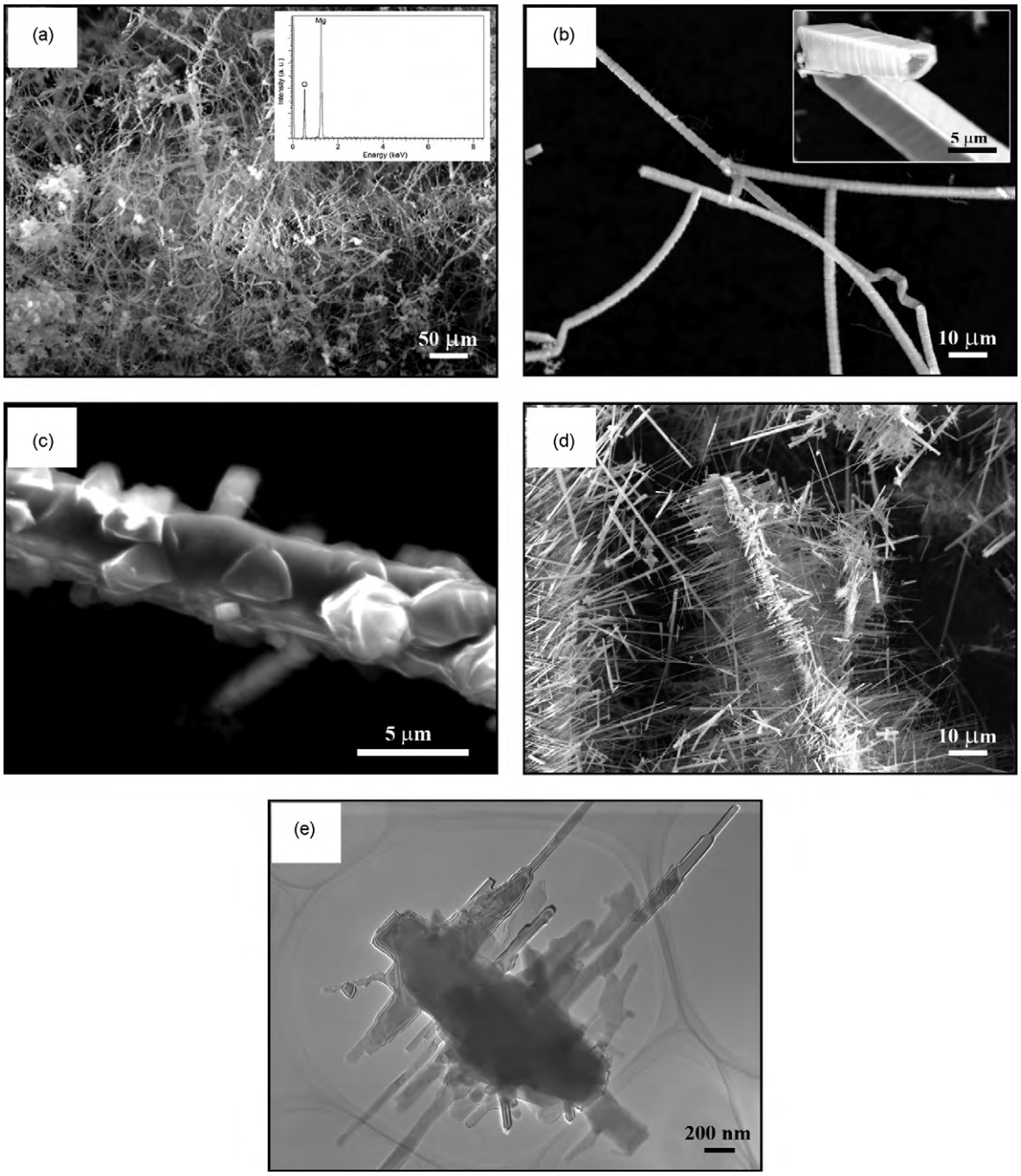

Fig. 6. (a) SEM image of the as-synthesized wool-like MgO fibers obtained from MG8 sample; inset: the corresponding EDS spectrum. (b) A typical high magnification SEM image of the shape characteristics of the MgO fibers; inset: a fiber with pyramid-shaped tip. (c) The SEM image of the camphor tree stalk-like fibers. (d) Branchy fibers with more than ca. 100 sub-branches attached to the stem, similar to fishbone or fern. (e) A typical TEM image of MgO fiber with sub-branches.

phologies we observed could be attributed to the variation in MgO concentration, and thus different levels of supersaturation. It is believed that different Mg vapor sources produced different Mg vapor concentrations, resulting in different fiber diameters and growth mechanisms.

The Mg vapor generated by carbothermic reduction is considered to be oxidized thoroughly at the central heating zone, and the following reaction can occur:

$$2Mg_{(g)} + O_{2(g)} \rightarrow 2MgO_{(s)} \quad (2)$$

The oxygen mainly originated from the oxygen in the carrying gas. Its supply was kept constant during the whole reaction. The MgO clusters formed are then transported to nucleation sites. It is easy to understand that there is a difference between the concentration of Mg vapor generated from different samples, i.e., during the carbothermic reaction (Reaction (1)), the concentration of Mg vapor generated by heating the intermediate activated sample (MG1) is smaller than that of Mg vapor generated by heating the more activated sample (MG8). It means by using more activated source material, higher level of supersaturation will be achieved. Hao et al. proposed various growth models under different supersaturation ratio in the preparation of MgO nanostructures [18,20]. Similar to that, at low supersaturation ratio, the surface diffusion rate of newly arriving clusters is high, and the relatively high substrate temperatures around 1000 °C guarantee that MgO clusters can migrate to high defect density sites (such as kinks, ledges, and

steps) and incorporate into lattices there to minimize the surface energy. During the persistent growth, the high defect density surface will become the rough growth front. The other four planes will gradually turn to side surfaces. Therefore, nanorods of high aspect ratio are formed in current experiments (Fig. 5).

In contrast, under high supersaturation ratio, more MgO clusters will arrive on the formed nuclei in the same time span. Thereby, the probability of surface migration will decrease and the growing tip can only consume a small amount of Mg vapor, and a large amount of Mg vapor will deposit on the surface of the grown fibers, making the grown fibers lengthen and thicken (Fig. 6).

The variation in the level of MgO supersaturation might also be responsible for the branching habit observed in the products (Fig. 6). Under further higher supersaturation ratios, in case of using more activated source material, a large quantity of clusters homogeneously adsorbs on the surfaces of MgO nuclei. However, high defect density sites on each facet of the nuclei incorporate more MgO clusters through surface diffusion and migration of these clusters and direct the growth of branches. During the process, the end parts of each branch dominate the growth due to higher defect density. Therefore, branched fibers are formed.

4. Conclusions

In summary, we have demonstrated a carbothermic route to synthesis of 1D MgO structures at a temperature (1000 °C) relatively lower than that required in previous approaches (≥1200 °C) that directly use MgO as the source material. The Mg vapor, generated by carbothermic reduction of MgO, subsequently reacted with trace O_2 contained in the reaction system and formed MgO vapor. Under appropriate conditions, the MgO vapor could reach supersaturation, condense onto the surface of a substrate that was placed on top of the source powder, and grow into highly anisotropic structures. The effect of the degree of mechanical activation on the morphology of MgO formed from the mechanically activated MgO and graphite mixture was investigated. The dependence of the MgO morphology on the degree of mechanical activation can be explained by the variation in the level of Mg vapor partial pressure and MgO supersaturation ratios. These phenomena are investigated and explained based on the increased reactivity of the reactants. As a result, two distinctive morphologies were found for MgO products: single crystalline nanorods with rectangular cross-sections whose diameters range from 50 to 100 nm, and microfibers (~5 μm in diameter) with and without branching. A mechanism based on the vapor–solid growth process is proposed for the formation of these morphologies. Source material with different degrees of mechanical activation affect the diameter and growth mechanism of MgO nanorods and microfibers by influencing the concentration of Mg vapor in the reaction tube.

References

[1] H. Yang, H. Al-Brithen, A.R. Smith, J.A. Borchers, R.L. Cappelletti, M.D. Vaudin, Appl. Phys. Lett. 78 (2001) 3860–3865.
[2] G.W. Wagner, P.W. Bartram, O. Koper, K.J. Klabunde, J. Phys. Chem. B 103 (1999) 3225–3228.
[3] Z.R. Dai, Z.W. Pan, Z.L. Wang, Adv. Funct. Mater. 13 (1) (2003) 9–24.
[4] P. Yang, C.M. Lieber, J. Mater. Res. 12 (11) (1997) 2981–2996.
[5] Y. Yin, G. Zhang, Y. Xia, Adv. Funct. Mater. 12 (4) (2002) 293–298.
[6] C. Tang, Y. Bando, T. Sato, J. Phys. Chem. B 106 (30) (2002) 7449–7452.
[7] Y.Q. Zhu, W.K. Hsu, W.Z. Zhou, M. Terrones, H.W. Kroto, D.R.M. Walton, Chem. Phys. Lett. 347 (2001) 337–343.
[8] J. Zhang, L. Zhang, X. Peng, X. Wang, Appl. Phys. A 73 (2001) 773–775.
[9] J. Zhang, L. Zhang, Chem. Phys. Lett. 363 (2002) 293–297.
[10] Y. Li, Y. bando, T. Sato, Chem. Phys. Lett. 359 (2002) 141–145.
[11] J. Zhan, Y. Bando, J. Hu, D. Golberg, Inorg. Chem. 43 (2004) 2462–2464.
[12] Y. Chen, J. Li, Y. Han, X. Yang, J. Dai, J. Crystal Growth 245 (2002) 163–170.
[13] Y.B. Li, Y. Bando, D. Golberg, Z.W. Liu, Appl. Phys. Lett. 83 (5) (2003) 999–1001.
[14] J. Jie, C. Wu, Y. Yu, L. Wang, Z. Hu, Nanotehnology 20 (2009) 1–6.
[15] K.L. Klug, V.P. Dravid, Appl. Phys. Lett. 81 (9) (2002) 1687–1689.
[16] Z. Zhou, S. Xie, D. Wan, D. Liu, Y. Gao, X. Yan, H. Yuan, J. Wang, L. Song, L. Liu, Solid State Commun. 131 (2004) 485–488.
[17] X.S. Fang, C.H. Ye, L.D. Zhang, J.X. Zhang, J.W. Zhao, P. Yan, Small 1 (4) (2005) 422–428.
[18] Y. Hao, G. Meng, Y. Zhou, M. Kong, Q. Wei, M. Ye, L. Zhang, Nanotechnology 17 (2006) 5006–5012.
[19] Y. Yan, L. Zhou, Y. Zhang, J. Phys. Chem. C 112 (2008) 19831–19835.
[20] Y. Hao, G. Meng, C. Ye, X. Zhang, L. Zhang, J. Phys. Chem. B 109 (2005) 11204–11208.
[21] R. Ma, Y. Bando, Chem. Phys. Lett. 370 (2003) 770–773.
[22] C.O. Husle, W.K. Tice, Nature 206 (1965) 79–80.
[23] A.H. Heuer, P. Burnett, J. Am. Ceram. Soc. 50 (1967) 627–628.
[24] G. Brooks, S. Trang, P. Witt, M.N.H. Khan, M. Nagle, JOM 58 (2006) 51–55.
[25] M. Nusheh, H. Fukuyama, H. Yoozbashizadeh, M. Askari, J. Kano, F. Saito, CAMP-ISIJ 22 (2009) 859–860.
[26] M. Nusheh, H. Yoozbashizadeh, M. Askari, N. Kuwata, J. Kawamura, J. Kano, F. Saito, H. Kobatake, H. Fukuyama, ISIJ Int. 50 (5) (2010) 668–672.
[27] J. Hu, T.W. Odom, C.M. Lieber, Acc. Chem. Res. 32 (1999) 435–445.
[28] W.B. Campbell, in: A.P. Levitt (Ed.), Whisker Technology, Wiley, New York, 1990, pp. 15–20.
[29] G.W. Sears, Acta Metall. 4 (1955) 361–367.